Nuclear Instruments and Methods in Physics Research A 609 (2009) 194–204

Contents lists available at ScienceDirect

Nuclear Instruments and Methods in Physics Research A

journal homepage: www.elsevier.com/locate/nima

Determination of correction factors for borehole natural gamma-ray measurements by Monte Carlo simulations

M. Maučec [a,b,*], P.H.G.M. Hendriks [a,1], J. Limburg [c], R.J. de Meijer [a,2]

[a] Nuclear Geophysics Division, Kernfysisch Versneller Instituut, Rijksuniversiteit Groningen, Zernikelaan 25 9747 AA Groningen, The Netherlands
[b] Reactor Physics Division, Jožef Stefan Institute, Jamova 39, 1001 Ljubljana, Slovenia
[c] Medusa Explorations B.V., Kadijk 7-B, 9747 AT Groningen, The Netherlands

ARTICLE INFO

Article history:
Received 31 January 2008
Received in revised form
30 July 2009
Accepted 14 August 2009
Available online 22 August 2009

Keywords:
Monte Carlo simulation
Natural gamma-ray spectrometry
Well logging

ABSTRACT

The analysis of natural γ-ray spectra measured in boreholes has to take into account borehole parameters such as the presence of casings and borehole diameter. For large, high-efficiency γ-ray detectors, such as BGO-based systems, which employ full-spectrum data analysis, corresponding corrections were not previously determined. In a joint project of the Nuclear Geophysics Division of the Kernfysisch Versneller Instituut (NGD/KVI), Groningen, Medusa Explorations B.V. and the Dutch Institute for Applied Geosciences (TNO-NITG) a catalogue of corrections was constructed. Using the Monte Carlo code MCNP, the influence of steel casings, borehole diameter, central axis probe position and the diameter of the γ-ray detector on the γ-ray spectra has been investigated for nearly 20 geometries. The calculated γ-ray spectra are compared qualitatively and quantitatively. In a case study, γ-ray spectra from a borehole measured in a cased and uncased configuration are analyzed with simulated spectra. When no corrections are used, the activity concentrations deviated by as much as 50% between the two measurements. Taking into account the specific measurement geometry, the activity concentrations were found to be identical within the statistical and systematic uncertainties of the experiment for the same borehole, with and without casing. These results illustrate the need for borehole-specific corrections and this study demonstrates that Monte Carlo methods are a fast and reliable way to calibrate well-logging tools for a wide variety of configurations.

1. Introduction

Borehole measurements provide information on the subsurface geology. The oldest use of nuclear techniques was based on measurements of γ-radiation emitted by the natural radionuclides ^{40}K, ^{232}Th and ^{238}U. Transitions between two formation classes were located based on changes in count rates.

When the individual activity concentrations of the natural radionuclides are known, even the formation composition can be extracted from the spectra of natural γ-radiation since they are characteristic for geological classes (e.g., sand or clay). In other words, the particular set of activity concentrations of ^{40}K, ^{232}Th and ^{238}U can be considered as a "fingerprint" of the soil composition [1,2]. If the radiometric fingerprints of the components of a formation are sufficiently different, it is furthermore possible to make a distinction between two variations of the same class (i.e. clay members kaoline and illite [3]). In the second half of the 1990s, improvements in both γ-ray detector technology and computers made it possible to derive, *quantitatively*, the individual radionuclide concentrations in a geological matrix from *in situ* γ-ray measurements and thus classify a formation based on measurements of natural γ-radiation.

The measured γ-ray spectrum is considered to be a combination of a background spectrum (e.g. from a stabilization source within a detection system) and the contributions of the activity concentrations of the natural radionuclides. This technique, the "Full Spectrum Analysis" (FSA) [4], derives the activity concentrations for each of the natural radionuclides by unfolding the measured γ-ray spectrum. Using the (nearly) full measured γ-ray spectrum in the analysis, the statistical uncertainties are reduced.

In the Full Spectrum Analysis (FSA) method, the measured spectrum $S(i)$ (normalized for measuring time) is regarded for each channel i as the sum over all radionuclides of standard spectra ($X_j(i)$) multiplied by the activity concentration C_j plus a background ($Bg(i)$) component:

$$S(i) = \sum_{j=1}^{M} C_j X_j(i) + Bg(i) \quad (1)$$

* Correspondence to: Halliburton/Landmark, 1805 Shea Center Drive, Suite 400, Highlands Ranch, CO 80129, USA. Tel.: +1 303 803 0327; fax: +1 303 488 3042.
E-mail address: marko.maucec@halliburton.com (M. Maučec).
[1] Present address: Gassco AS, Haugesund, Norway.
[2] Present address: Stichting EARTH, de Weehorst, Peize, The Netherlands.

0168-9002/$ - see front matter © 2009 Elsevier B.V. All rights reserved.
doi:10.1016/j.nima.2009.08.054

The index j runs from 1 to M, representing the number of radionuclides. A standard spectrum represents the response of the detector in a given geometry to activity concentration of 1 Bq/kg of a given radionuclide.

If for a certain geometry the standard spectra X_j and the background spectrum are known, a measured spectrum $S(i)$ can be analyzed with the standard spectra by the procedure that finds the best C_j values and minimizes χ^2, a measure of the discrepancy between the measured spectrum and the calculated spectrum. The standard spectra for the individual radionuclides, $X_j(i)$, are determined from measurements of samples with well-known activity concentrations. Because the samples will contain trace elements of more than one radionuclide, their concentrations combined give the activity concentration matrix, M. The calibration spectra, CS, are measured for each calibration sample. The standard spectra X then follow from the matrix equation $[CS] = [M] \times [X]$ and are calculated by inverting the concentration matrix M in $[X] = [M]^{-1} \times [CS]$.

Borehole characteristics such as the borehole diameter and the presence of casing material influence the shape and intensity of the measured γ-ray spectra. As a result *quantitative* data can be extracted only if calibrations are available for the particular field conditions.

To circumvent these issues, mineral (uranium) and petroleum exploration/exploitation industries have pioneered development of techniques for borehole and casing corrections of spectral γ-ray logs since the early 1980s. Evans and Wilson [5], for example, produced simulated correction curves for centered and side-walled KUT tools, using the Department of Energy (DOE) energy windows. Furthermore, Koizumi et al. [6] have derived corrections for a steel borehole casing and a diameter of a water-filled borehole from contaminant-assessment measurements with calibration standards for an HPGe detector system, while Stromswold and Wilson [7] have generated similar correction factors to assay for uranium ore with KUT probes. In [8], Koizumi introduces the derivation of environmental corrections for a natural spectral γ-ray logging system through computer modeling calculations using analog Monte Carlo code GAMRES [9], originally developed by Evans, to calculate scintillation detector response functions. However, the efforts to assess the borehole logging tool correction factors are not limited only to natural γ-ray (KUT) spectrometry. Koizumi [10] utilizes DOE passive γ-ray calibration standards to calculate correction factors for shallow subsurface Pulsed Neutron Capture (PNC) logging tool equipped with HPGe detector, while Mickael et al. [11] account for variations in completion geometry, borehole diameter and formation porosity and mineralogy in dual-detector carbon/oxygen (C/O) logging. In the late 1990s Monte Carlo (MC) simulations of radiation transport became increasingly popular as a benchmark and calibration tool for nuclear logging sondes. Odom et al. deployed MCNP [12] and GAMRES [9] to model detector response functions to γ-rays, induced by thermal neutron capture and inelastic scattering of fast neutrons [13] and to model the depth of investigation and cased-hole well-bore uncertainties [14], while Michael developed MC-based algorithm to correct PNC decay logs for borehole and diffusion effects [15].

Typically, the response of well-logging equipment is calibrated in test pits in which the elemental composition, activity concentrations and lithology are known [16]. These test facilities consist of pits with several diameters and contain cased and uncased intervals. An overview of available test facilities is given by Arnold and Butler [17]. The results of the pit-calibrations are extrapolated to field conditions using departure curves to correct for factors such as tool eccentricity, borehole diameter and mud-cake thickness. The compiled data are published by manufacturing and vendor companies for the use in data analysis (e.g. *"Log Interpretation Charts"* by Schlumberger [18]). This approach, however, has several disadvantages. Firstly, all major test pits (such as those approved by the American Petroleum Institute, API) are in the USA. This makes calibration of new detector systems expensive and impractical. Secondly, even after extrapolation, the test facilities only cover a limited number of combinations of drill systems and lithology.

Although most correction functions available in the open literature are energy and nuclide independent and thus do not take into account changes in spectral shape, Koizumi et al. [6] derived source- and energy-dependent environmental corrections and calibration factors for the three-window KUT analysis of spectral γ-ray logging data. Unfortunately, for novel spectrometry tools, which employ large, high-efficiency BGO detectors and FSA, the available correction factors are too limited, thus imposing the need for the study outlined in this paper.

In a joint project of the Nuclear Geophysics Division of the Kernfysisch Versneller Instituut (NGD/KVI), Groningen, Medusa Explorations B.V. and the Dutch Institute for Applied Geosciences (TNO-NITG), a catalogue of corrections for natural γ-ray measurements in boreholes is constructed. This correction catalogue accounts for the effect of the following parameters on measured γ-ray spectra:

1. presence of steel borehole casings;
2. borehole diameter;
3. probe central axis position;
4. dimension of the γ-ray detector.

In practice, a vast number of combinations of these parameters occur, too large to be covered by experimental set-ups. In this work, the detector calibration is done by means of Monte Carlo (MC) simulations. Furthermore, the inclusion of environmental corrections is tested in a case study in which experimental γ-ray spectra are analyzed from a borehole that has been measured with and without the presence of casings.

2. Modeling aspects

2.1. Borehole configurations

For boreholes up to 100 m deep, the most commonly used drilling technique for unconsolidated sediments is the so-called *pulse-drilling* technique, where a stainless-steel casing is pushed into the ground by applying a pulsating pressure on the casing. For a given casing diameter, the maximum depth is approximately 30–35 m. For deeper holes, additional casings with a smaller diameter are inserted to pulse the next 30 m. Therefore, for boreholes deeper than 30–35 m, each stage of the borehole differs in diameter and the number of casings. As a consequence, the absorption of radiation by the borehole constituents (fluid, clays and casings) differs for the stages. The simulated configurations are listed in Table 1 and schematically depicted in Fig. 1: open-central, open, one-, two- and three-casings and side-walled (note: "two-casings" and "side-walled" geometries are the same, except for the detector/housing diameters). A listing of the material properties is given in Table 2. It is established from auxiliary simulations that a formation of 50 cm thickness reproduces the total intensity of an infinite bed within 98.6% [19]. This is in agreement with experiments where an equivalent infinite thickness of 50 cm was found for a density of 2.25 g cm^{-3} [20]. In this work and throughout this document, it is assumed that the borehole is filled with fresh water.

The energy-resolution for the BGO detector with a crystal diameter of $\varnothing$5.0 cm was extracted from measurements and

Table 1
Simulated configurations for various borehole diameters are indicated with an "X".

Borehole diameter (cm)	Open hole	1 casing	2 casings	3 casings	Side-walled[a]
7	X				
15.24	X				X
17.8	X	X			
21.9	X	X	X		
26.7	X	X	X	X	
32.4	X	X	X	X	
50	X				
100	X				

[a] *Note*: "2 casings" and "side-walled" geometries are the same, except for the detector/housing diameters.

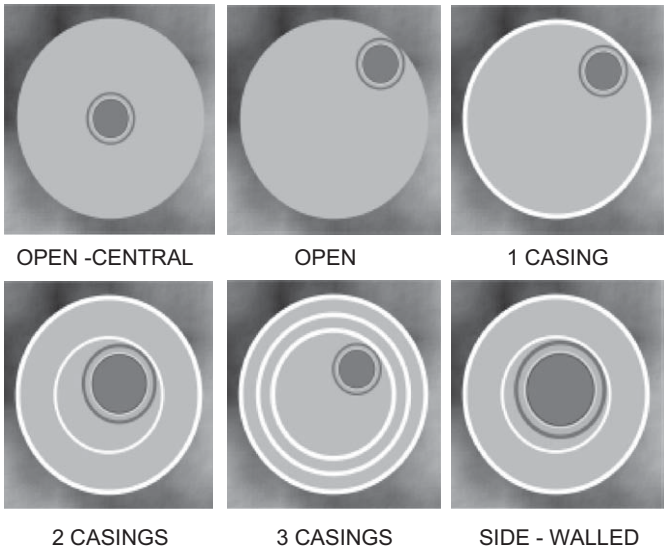

Fig. 1. Top view of the simulated borehole configurations. The first five images schematically show various cased configurations as they appear for several diameters. The casings (white) are steel and have a thickness of 7.5 mm. The last image represents the side-walled configuration, which only exists for a 15.24 cm borehole diameter and with an inner casing thickness of 2.5 mm. Generally, a detector is located against the formation (or casing), but situations in which the detector is located at other axial positions do occur. Detectors with two crystal diameters, ∅3.8 and ∅5.0 cm, were modeled in this work. Note: "2 casings" and "side-walled" geometries are the same, except for the detector/housing diameters.

Table 2
Listing of the materials used in the simulations.

	Thickness (mm)	Material	Density ($g\,cm^{-3}$)
Casings	7.5[a]	Stainless steel 347	7.92
Detector			
Scintillator crystal	∅50 length 150	BGO ($Bi_4Ge_3O_{12}$)	7.13
Reflector	3	Teflon (CF_2)	2.175
Silicon rubber	1	G.E. RTV12A	1.019
Crystal housing	0.8	Aluminum	2.70
Pressure housing	3.25	Stainless steel 347	7.92
Water	N/A	Hydrogen [11.2%] Oxygen [88.8%]	1.00
Air	N/A	Oxygen [23.2%] Nitrogen [75.5%] Carbon [0.1%] Argon [1.3%]	1.13×10^{-4}
Soil	500	Mixture of SiO_2 and H_2O	2.15

[a] Except for the inner casing of the side-walled configuration, which is 2.5 mm thick.

found to be 8.1% at 1.3 MeV at room temperature. A similar detector system with a crystal diameter of ∅3.8 cm was simulated as well (see Section 4.3).

3. Monte Carlo approach

The Monte Carlo radiation transport code MCNP4C [12] was used for all simulations running on one or more PC nodes. To speed up the computations, the time-consuming electron transport in regions far from the detector was omitted and a true physical model was used closer to the detector [21]. In addition, direction and starting location of particles were biased, yielding the reduction of computation time per simulation as well as of the statistical uncertainty by factors seven and three, respectively [21].

The geological formation in the simulations is assumed to be homogeneous in composition and radionuclide activity concentration. Three source models are made, one for each of the three natural radionuclides ^{40}K, ^{232}Th and ^{238}U. Each source model includes all discrete γ-ray emissions (single line for ^{40}K, 346 and 458 lines for ^{232}Th and ^{238}U decay series, respectively) and their associated emission probabilities as given by their decay scheme according to [22]. The validity of the simulated γ-ray spectra has been verified in a benchmark study [21]. Comparison between standard spectra from experiments and simulations for ^{40}K, ^{232}Th and ^{238}U is given in Fig. 2. Overall, an excellent agreement between experimental and simulated data is obtained. The only notable mismatch occurs in continuum intensity for ^{40}K spectra. It is likely to be attributed to systematic error in the experimental data, caused by the incomplete removal of background radiation from concrete surroundings of calibration drums and by the "cross-talk" between the measured spectra in the unfolding procedure to standard spectra. For ^{232}Th and ^{238}U the model and experiment agree within 6% and differences are caused by the systematic uncertainty in the experiments, such as density variations in the uranium-enriched drum.

The Monte Carlo simulations are deployed to calculate two quantities: (1) the γ-ray flux over a detector using a track-length estimator and (2) the pulse-height spectra, acquired by an energy deposition estimator. By considering both the photon flux and pulse-height spectra over a detector, it is possible not only to quantify the effects of the various parameters but also to understand the causes for their occurrence.

4. Results

For each of the investigated parameters, an assessment is made of the energy- and radionuclide-dependence, as well as the magnitude of induced intensity-variations. The effects are presented for a formation containing only the naturally occurring mono-energetic γ-ray emitter ^{40}K. The same effects occur in the thorium and uranium spectra, but due to the large number of γ-rays emitted in corresponding decay series, the effects interfere and the picture becomes less transparent. With more than 300 γ-rays per decay series, there is no longer a pure continuum and the distinction between photo-peak area and continuum disappears.

4.1. Effects of borehole casing(s)

First, the influence of the detector is "switched off", i.e., only the photon flux over the detector is considered without calculating the energy deposition in the crystal. The example is calculated for a 26.7-cm-diameter borehole with the detector located against the casing or formation wall. The left-hand panel of Fig. 3 presents

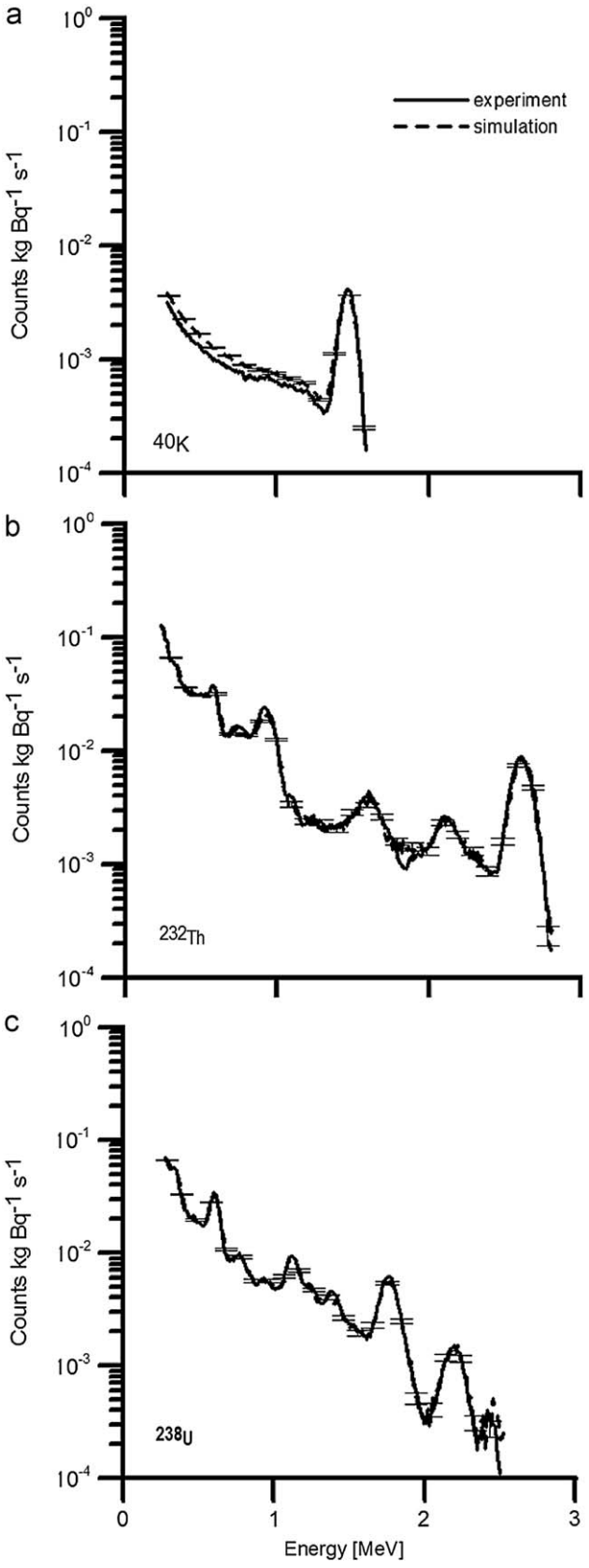

Fig. 2. Comparison between borehole standard spectra from experiments (solid line) and simulations (dashed line) for (a) ^{40}K, (b) ^{232}Th and (c) ^{238}U. The statistical uncertainty (1σ) for the experimental data is smaller than the size of the marker. For the simulated data the statistical uncertainty is given for every 100 keV. The γ-ray intensity (vertical axis) is given on a logarithmic scale. Due to an overall excellent agreement between experimental and simulated spectra in intensity as well as the shape, the dashed and solid lines appear difficult to distinguish.

the photon flux at the location of the detector as a function of energy for a number of casings. All fluxes are normalized with respect to the bare borehole situation. Next, the detector effects are "switched on" and the γ-ray spectra are considered for four configurations. The results are shown in Fig. 4, which indicates that the effect of the detector with its finite energy-resolution predominantly causes a smoothing of the spectrum, mainly determined by the transport of γ-radiation prior to reaching the detector.

The effect of the casings on the γ-ray spectra is mainly an intensity reduction as shown in Figs. 3 and 4 and requires a correction factor for the continuum and the photo-peak. The average reduction may be determined in the typical energy range that is used when the γ-ray spectra are analyzed for activity concentrations, i.e., $0.35\,\text{MeV} < E_\gamma < 2.85\,\text{MeV}$. The average is weighed using the statistical uncertainties in the bin intensities. The average reductions are given in Fig. 5 as a function of the number of casings. By removing the energy dependence of the intensity reduction, a systematic[3] error is introduced, given by the standard deviation ($s_{\hat{x}}$) of the weighted average ($\hat{x}$):

$$s_{\hat{x}} = \left(\sqrt{\sum_{i=1}^{n} \frac{1}{\sigma_{wi}^2}} \right)^{-1} \tag{2}$$

where σ_{wi} represents the standard deviation that accounts for the spread between the energy-independent parameter x_i calculated for different configuration i (σ_{xi}) as well as the contribution from the Monte Carlo statistical uncertainty (σ_{MCi}) and is defined as $\sigma_{wi} = \sqrt{w_i \sigma_{xi}^2 + (1 - w_i)\sigma_{MCi}^2}$. Here $w_i = \text{Counts}_{xi}/\text{Counts}_{xref}$ represents the weighting factor, calculated as the ratio between the count-rate corresponding to the parameter i vs. the reference parameter (e.g. borehole diameter). These systematic uncertainties are indicated as error bars in Fig. 5.

From Fig. 3 one notices that the reduction in flux is largest at the photo-peak energy and at $E_\gamma < 0.5\,\text{MeV}$. This result can qualitatively be understood by considering:

1. At the photo-peak energy, the γ-rays reach the detector without an interaction in either the formation or the casing and the fluid. Adding casings and fluid therefore enhances the chances for interaction and reduces the energy of the photon. At $E_\gamma = 1.46\,\text{MeV}$, the most likely interaction between the γ-ray and the media it traverses is Compton scattering, which gives rise to an event in the continuum part of the spectrum. Consequently, the photo-peak area is reduced more than the continuum part.
2. The photons at $E_\gamma < 0.5\,\text{MeV}$ are predominantly due to multiple scattering in the (multiple) casings and the borehole fluid (i.e. water). Moreover, in comparison to the formation, with $Z \approx 11$, the photoelectric cross-section for iron with $Z = 26$ is much higher in this energy range.

The scaling factors from Fig. 5 indicate that the effect of adding casings is exponential. For instance, one casing reduces the original ^{232}Th γ-ray intensity by 0.76, two casings by $(0.76)^2 = 0.58$ and three casings by $(0.76)^3 = 0.45$. Since each extra casing reduces the photon flux by the same factor, the three curves in the right-hand panel of lines of Fig. 3 cannot be distinguished.

This exponential behavior is expected since the transmission T of γ-radiation through matter is given by Lambert–Beers's law:

$$T(d) = e^{-\mu\rho d} \tag{3}$$

[3] The uncertainty is classified as "systematic" since the error is correlated to removing the energy dependence from intensity reduction.

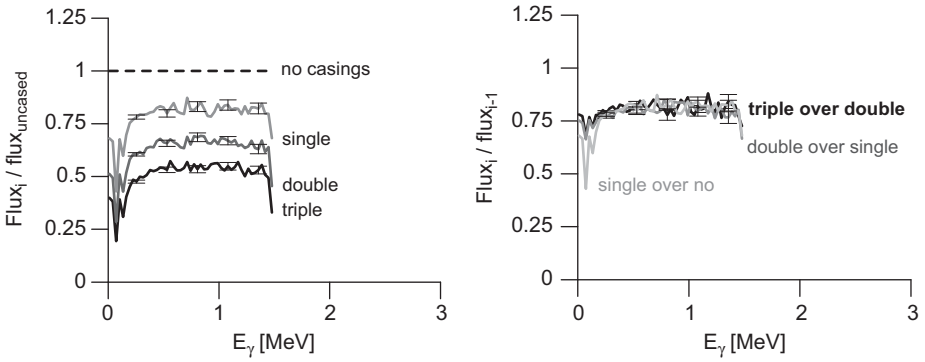

Fig. 3. *Left panel*: The relative photon flux over a detector in a 26.7-cm-diameter borehole for one-, two- and three-steel casings is given, relative to a configuration without casings. *Right panel*: Photon flux-reduction over a detector per additional steel casing. For both figures, the statistical uncertainties are given every 100 keV and the source is ^{40}K.

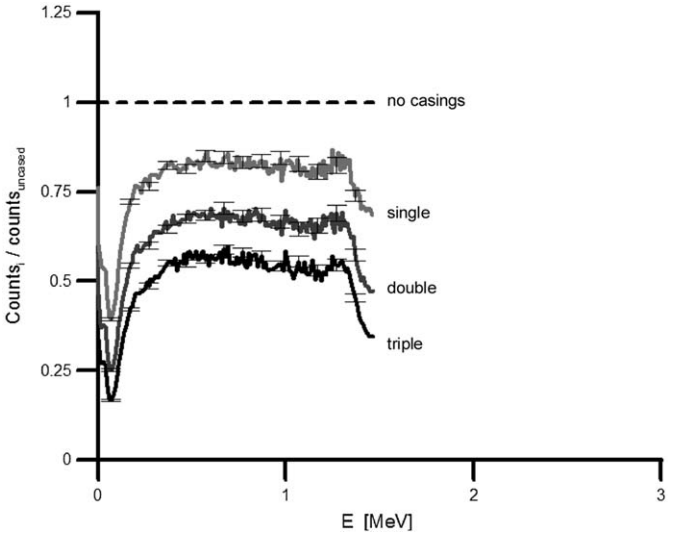

Fig. 4. The relative intensity of simulated ^{40}K γ-ray spectra for a borehole with three casing configurations is given, relative to a configuration without casing. Statistical uncertainties are given every 100 keV. The borehole diameter is 26.7 cm.

with d being the thickness of the absorber, ρ its density and μ the mass attenuation coefficient. Transmission T is usually referred to as I/I_0, representing the ratio of the outgoing vs. the incident intensity of γ-radiation. In general, Lambert–Beers's law represents an elementary formula, valid for the passage of mono-energetic γ-rays through a fixed scatterer with a small angular distribution about the main incident direction. In the present case, the small deviation from a pure exponential reduction is caused by the fact that the extra shielding from each additional casing is accompanied by extra shielding from borehole fluid between the casings.[4] Furthermore, the variable penetration depth in the formation, combined with the wide-angle scattering, gives rise to build-up factor B. Lambert–Beers's law is then corrected as $T(d) = Be^{-\mu\rho d}$, where B is unity for small angle conditions and otherwise >1.

If γ-ray spectra are analyzed by merely using energy-independent reductions (rather than using configuration-specific standard spectra) the inferred systematic uncertainty in the calculated activity concentrations is in the order of 8%. Using standard spectra that specifically correspond to the borehole configuration in which the data are acquired, this additional uncertainty in the activity concentrations is avoided.

4.2. Effects of borehole diameter

The selection of the borehole diameter is, amongst others, determined by the desired final depth of the borehole. As the borehole diameter increases, the spectral intensity decreases, because the detector is located against an uncased borehole wall and less radiation from the opposite side of the borehole reaches a detector. As an extreme case, a ∅7 cm detector housing in a 7-cm-diameter borehole is considered. In this situation, the detector housing is in full contact with the formation and no fluid is present. The standard spectra for the different borehole diameters are given in Fig. 6, relative to the 32.4-cm-diameter borehole. Intuitively, probability for γ-ray scattering (and hence energy loss) increases with the distance between formation and detector and therefore with the borehole diameter. For a 7-cm-diameter borehole (i.e. no fluid) the effects of multiple scattering are smallest, yielding a relatively high flux at photo-peak energies and low flux of multiple scattered radiation.

To quantify the intensity reduction due to an increasing borehole diameter, the intensity reduction is approximated by an energy-independent factor. This approach is similar to the assessment of reduction factors for borehole casings. Herewith, the reduction curves for ^{40}K, ^{232}Th and ^{238}U (such as the ones presented in Fig. 6) are fitted for the energy window $0.35\,\text{MeV} < E_\gamma < 2.85\,\text{MeV}$. The results are shown in Fig. 7, presenting the simulated intensity of the γ-ray spectra of the natural radionuclides, relative to a borehole diameter of 7.0 cm for several borehole diameters.

The intensity reductions as outlined in Fig. 7 show an exponential decay, $e^{-\mu\rho d}$, similar to the effect of the casings in Fig. 5. The lower value of the intensity reduction reflects the lower density of the water relative to steel, while the smaller effect of borehole diameter on ratio (relative to the casing) is also due to geometry difference. For the casing, the attenuator is between the source and the detector, while for the water the source is next to the detector at contact location, regardless of diameter.

Fig. 7 shows that for small borehole diameters (<25 cm), the slope of the curve is steep. This indicates that for small boreholes, the variations in borehole diameter along the borehole have a large influence on the absorption. Moreover, if the borehole diameter goes to infinity, the reduction factor will asymptotically approach a constant value, corresponding to underwater, flat-bed spectra. This limit is shown as a reference in Fig. 7 and equals to

[4] In Ref. [7], Stromswold and Wilson also report exponential behavior with thickness for casing attenuation measurements of KUT logging tools. However, they found the attenuation coefficients for steel casing to be ~40% higher than handbook values for the used DOE energy windows. This was attributed to the effect of average angle of incidence of non-scattered source γ-rays from the formation being in average 45° different from those for the reference geometry attenuation.

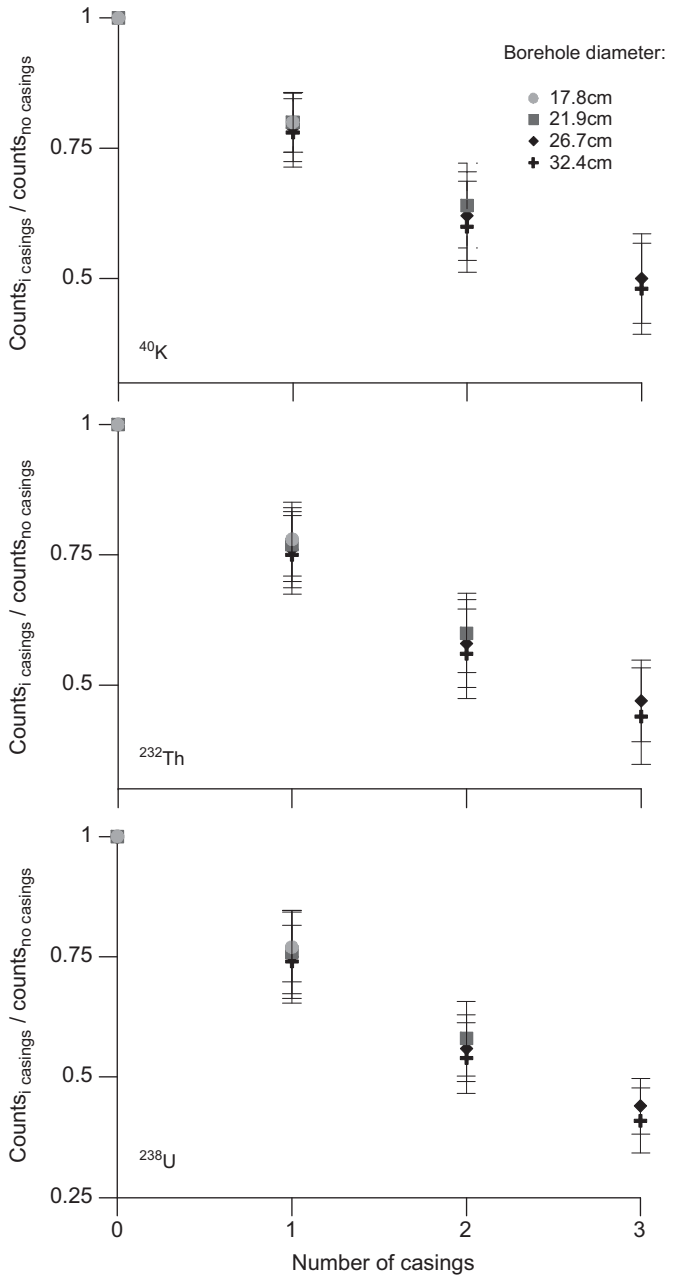

Fig. 5. Average casing energy reduction factors per nuclide for various borehole diameters. The uncertainties are systematic (i.e. derived by Eq. (2) in Section 4.1) and are induced by assuming γ-ray energy-independent reductions.

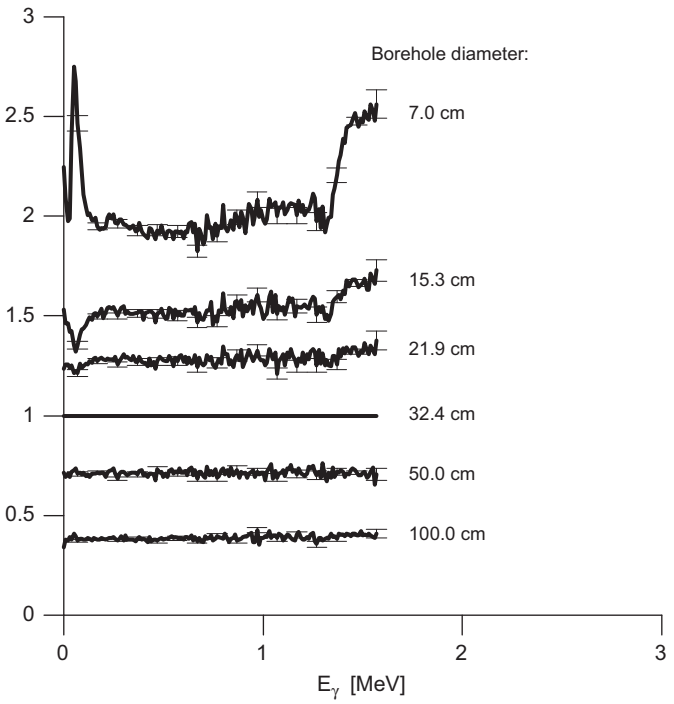

Fig. 6. Relative pulse-height intensities for selected borehole-diameters with respect to a 32.4-cm-diameter borehole. Statistical uncertainties are given every 100 keV; the γ-ray source is ^{40}K.

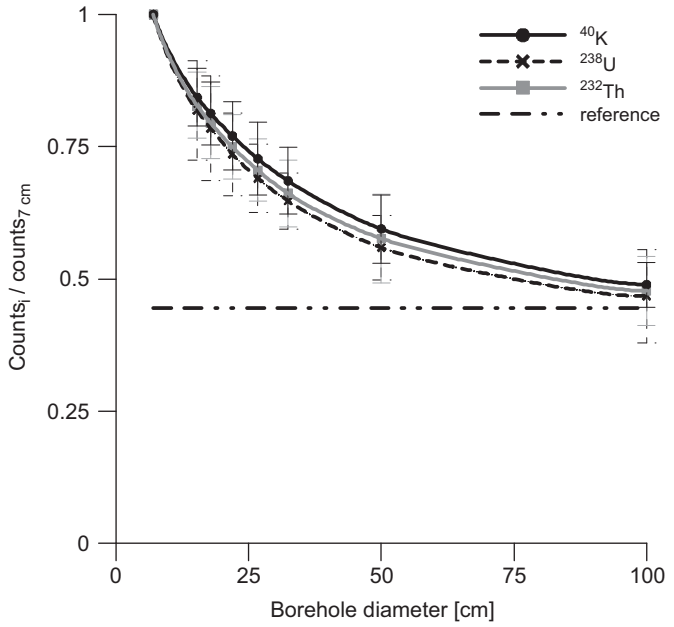

Fig. 7. Spectral averaged intensities for various borehole diameters with respect to a 7.0-cm-diameter borehole. The data points are connected by a smooth spline. The dash-dotted line corresponds to the (asymptotic) reduction factor for an infinite diameter borehole as derived in Ref. [23]. The uncertainties are systematic (i.e. derived by Eq. (2) in Section 4.1) and are introduced by assuming γ-ray energy-independent reductions.

0.45, as derived in Ref. [23]. Again, by approximating the energy-*dependent* curves such as given in Fig. 6 by an energy-*independent* factor, a systematic uncertainty of the order of 10% is introduced.

Based on the γ-ray intensity reductions as a function of borehole diameter, it is possible to infer qualitatively what the effects of changes in borehole fluid density are. In this work it is assumed that the borehole is filled with fresh water. In practice, often additives such as bentonite[5] are used, which increases the density of the borehole fluid by approximately 5%. Neglecting the effect of changing μ due to the change in Z in a mixture of bentonite and fresh water is roughly equivalent to a 5% increase in borehole diameter (Eq. (3)). Fig. 7 shows that the effects of a 5% increase in borehole diameter on the measured γ-ray intensity are negligible. However, the strong Z dependence on the attenuation is important only at low energies and becomes dominant as

[5] A clay-like compound consisting of 69% SiO_2, 17% Fe_2O_3, 11%Al_2O_3 and several smaller fractions of miscellaneous oxides. Amongst others, the resulting borehole fluid has better properties concerning cooling and lubrication of the drilling bit. The activity concentrations of pure bentonite are typically 400 Bq/kg, 25 and 25 Bq/kg, for ^{40}K, ^{232}Th and ^{238}U, respectively.

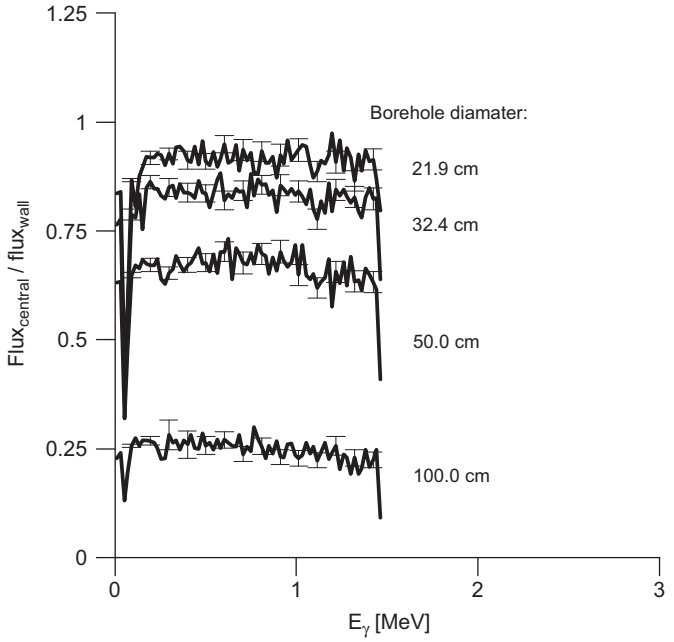

Fig. 8. The photon flux over an axially centered detector with respect to a detector located against the wall of an open borehole. The ratios are shown for several borehole diameters. Statistical uncertainties are given every 100 keV; the source is the γ-radiation emitted by decaying ^{40}K.

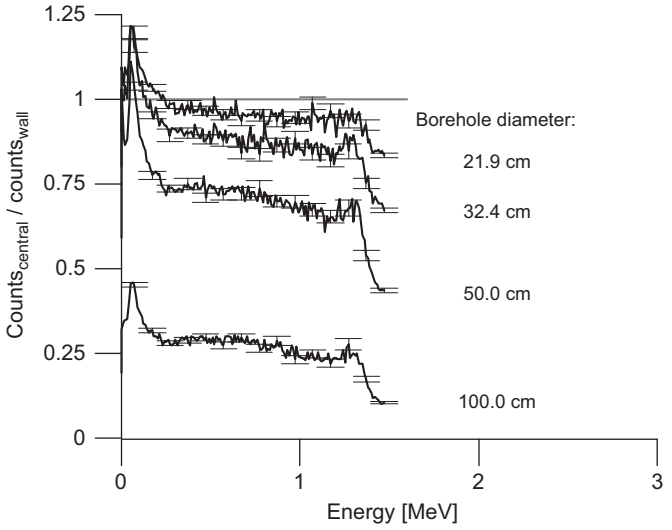

Fig. 9. The pulse-height intensity for an axially centered detector relative to those of a detector located against the wall of an open borehole. The intensity ratios are given for several borehole diameters. The source only contains the natural radionuclide ^{40}K. Statistical uncertainties are given every 100 keV.

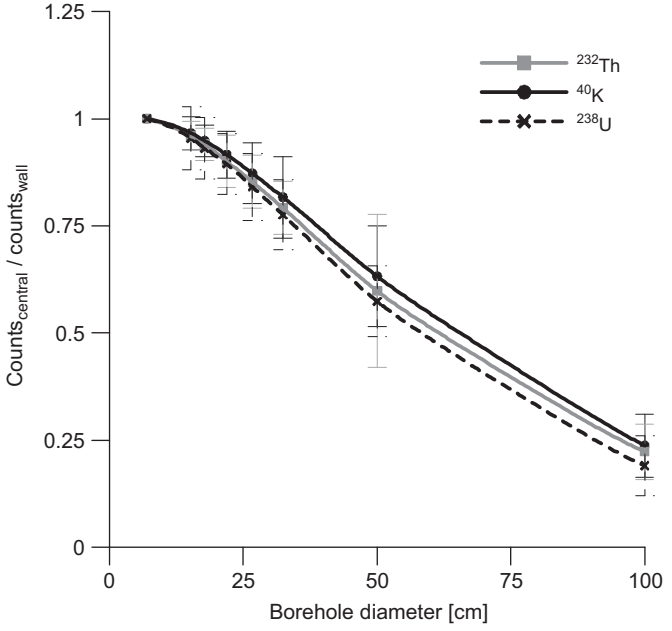

Fig. 10. Gamma-ray intensity reduction if a γ-ray detector is moved from a position against the borehole wall to the centre of an uncased borehole. The uncertainties are systematic (i.e. derived by Eq. (2) in Section 4.1) and are introduced by assuming γ-ray energy-independent reductions.

composition includes high Z elements. There are other borehole fluid additives that would have high Z effect, such as barium in barite added to drilling mud for weight; however, they were not considered in this work. Another effect is attributed to activity concentrations of ^{40}K, ^{232}Th and ^{238}U in a water/bentonite mixture. These concentrations are significant and should be included as a source of background radiation (i.e., radiation not originating from the formation of interest) in the analysis of borehole γ-ray spectra.

Generally, all boreholes exhibit a certain inclination with depth, which makes a detector lean against the formation wall (or casing). However, it is possible that a detector is not fully in contact with the borehole wall, for instance at shallow depths in large boreholes. Therefore, the influence of radial placement of a detector in a borehole is investigated. For this purpose, an additional configuration is simulated in which a detector is located in the centre of the borehole. This configuration induces the maximum change in the detector's response with respect to a detector located against the borehole wall. For these simulations, open (uncased) borehole configurations are assumed. A selection of the data, with a formation containing only ^{40}K, is given in Fig. 8. It compares the relative photon flux over a detector positioned in the centre of an uncased borehole to that of a detector located against the wall of the borehole. These results indicate that the overall photon flux is reduced if the detector is moved towards the centre of the borehole. Fig. 9 represents a detection ratio (i.e. ratio of counts from the pulse-height tally) and shows the relative γ-ray intensity for an axially centered detector with respect to a detector located against the wall of an open borehole. The intensity ratio is given for several borehole diameters.

The reduction curves in Fig. 9 are energy-dependent. However, to roughly quantify the effect of probe positioning, the curves are approximated by an energy-independent factor. Once more, this approach is similar to an approximation of the effects of borehole diameter and the number of casings. Therefore the same energy window is used for the approximation. The results are given in Fig. 10. The error bars in Fig. 10 ($<10\%$) represent the systematic uncertainty introduced by using an energy-independent intensity reduction. The derivation of such systematic error as the weighted average is given with Eq. (2) in Section 4.1.

Fig. 9 shows the relative γ-ray intensity for an axially centered detector with respect to a detector located against the wall of an open borehole. The intensity ratio for the γ-ray spectra as given in Fig. 9 demonstrates a dip in the photo-peak intensity, a rather flat continuum at intermediate energies and a relatively intense low-energy continuum, peaking at $E_\gamma < 200$ keV. Notably, Fig. 8 (flux calculations, indicating a dip at $E_\gamma < 200$ keV) and Fig. 9 (pulse-height spectra) cannot be compared directly, due to the different principles by which these quantities are estimated, cf.

[12]. Namely, this apparent discrepancy is caused by the different MC estimator, used to determine the flux and pulse-height spectra. In the assessment of photon flux, every γ-ray track crossing the detector[6] contributes to tally (spectrum) estimate, regardless of whether they are the progeny of the same source particle. For the estimation of the pulse-height spectrum, all tracks originating from the same source particle are combined and the *total* energy deposition is recorded. In other words, detected counts within a particular energy bin are due to corresponding γ-rays as well as γ-rays of higher energy that are Compton scattered in the detector and produce the energy deposited pulse, within the same energy bin.

As the borehole diameter increases, so does the absorbing layer between the detector and the source and hence the measured intensity decreases. The fact that the approximated curves in Fig. 10 are nuclide-specific curves is once again related to the energy characteristics of the sources. The mono-energetic γ-ray energy emitter ^{40}K indicates a smooth intensity reduction with borehole diameter, due to Compton-scattering effects. For ^{232}Th and ^{238}U, the region of interest for interpretation contains photo-peaks, which are greatly reduced in intensity. This explains the slight concave curvature around 50 cm in borehole diameter. For smaller diameters, the photo-peaks still contribute. Above 50 cm their contribution vanishes rapidly.

Extrapolating the curves in Fig. 10[7] until the γ-ray intensity is reduced to zero yields diameters of approximately 130, 130 and 125 cm for potassium, thorium and uranium, respectively. These numbers are *absorber* thicknesses, and represent the approximately 100% γ-ray shielding by the borehole fluid.

The product of density and thickness of the steel casings is equivalent to 15 cm of water. Moreover, in the 3-casing configuration, 6.8 cm of water is present between the formation and detector, in total adding to 22 cm of "water". To achieve an absorption by borehole fluid alone, equivalent to three casings, a water thickness of approximately 25 cm is needed (i.e., a borehole diameter of 56 cm, including the detector thickness, see Fig. 10). Hence, the high Z components in steel also lead to increased γ-ray absorption in the casings. This result indicates that processes other than Compton scattering are of importance as well.

Central axis positions of a detector occur mostly for shallow depths in wide boreholes, because here the hole is still vertical and a detector has not yet drifted towards the borehole wall. As seen in Fig. 10, especially for such wide boreholes, the intensity of the γ-ray spectra (and thus the uncertainty in derived activity concentrations) is strongly influenced by the probe location. Therefore, it is preferred to actively position the detector against the borehole wall while measuring, rather than correcting, for an axially drifting system in the data analysis. Such systems, e.g., using springs, are already employed in Neutron Gamma Activation tools, such as Pulsed Neutron Loggers [24].

4.3. Detector dimensions

For typical shallow-borehole measurements, BGO detectors are employed with a length of 15 cm and diameters of 5 or 3.8 cm. For both detector diameters, γ-ray spectra are simulated in an open 7-cm-diameter borehole for a formation that only contains ^{40}K. Both configurations include pressure housing with detectors axially centered in the borehole.

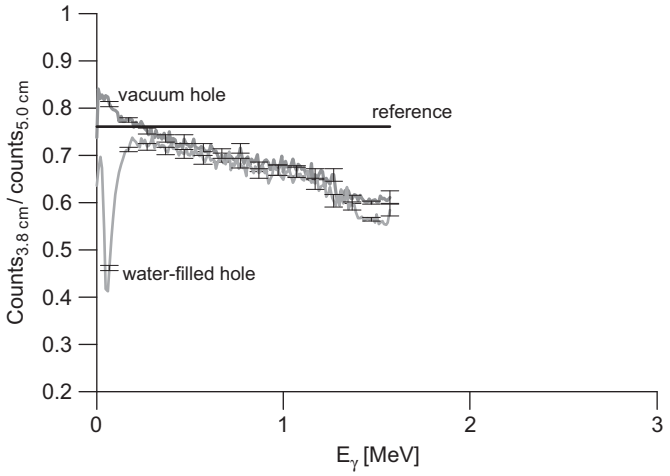

Fig. 11. Gamma-ray spectra intensities for BGO scintillation detectors of 15 cm length and diameters of 5 and 3.8 cm, respectively. Intensities are shown relative to the intensity as recorded in the 5-cm-diameter detector. Ratios are shown for a vacuum-filled and a water-filled borehole. Statistical uncertainties are given every 100 keV.

To investigate the effect of detector size, two simulations are carried out.[8] In the first simulation, the detectors are placed in a vacuum borehole. In the second, the detectors are placed in a water-filled borehole. For both simulations, the intensity of the γ-ray spectrum measured with the ∅3.8 cm detector is given relative to the ∅5.0 cm detector in Fig. 11. Assuming cylindrical symmetry, the area of the small detector is 0.76 times the area of the ∅5.0 cm detector. Ignoring multiple-scattering events in the detectors (i.e. considering the detector as opaque to incident γ-rays, that is, neglecting those passing through detector volume without interaction), this ratio represents the upper limit of the intensity ratio measured in the two detectors; this line is plotted as a reference in Fig. 11.

Three effects cause the spectrum ratios as seen in Fig. 11:

- The first effect is a decrease in γ-ray intensity with decrease in solid angle of a detector. This effect is independent of γ-ray energy and can be studied by "switching off" interactions in the borehole fluid. This is accomplished by filling the borehole with vacuum.
- The second effect is that the probability for γ-ray interaction with the detector material decreases with the detector volume traversed by the γ-ray. For low γ-ray energies, both detectors are sufficiently thick to fully absorb the γ-radiation, and the intensity ratios will be close to the upper limit given by the ratio of cylinder areas 0.76, as given before. As E_γ increases, the relative intensity in the ∅3.8 cm detector reduces. This corresponds to the declining intensity ratio as seen in Fig. 11. For 1.46 MeV, an intensity ratio of 0.58 is found, which is equal to the volume ratio of the two detectors. For $E_\gamma < 0.18$ MeV, the γ-ray intensity in the ∅3.8cm detector is higher than the upper limit, due to a higher rate of partial detections.
- Similar to the other two, the third effect is that the response of a γ-ray detector depends not only on detector characteristics but also on the γ-ray flux over the detector. By changing the detector dimensions, the photon flux over the detector is also changed. One manifestation of this effect is that the

[6] Assuming the use of track-length estimator.

[7] Presented curves (i.e. energy independent ratios) are similar to the inverse of the water correction factors modeled by Evans and Wilson [5], for a different type/size of detector. They used discrete ordinates to model flux at the detector surface, with high precision, and Monte Carlo code GAMRES [9] to model detector response to each incident energy and direction. They summed responses for the appropriate KUT energy windows.

[8] For the ∅3.8 cm detector no benchmark data are available. It is assumed that the characteristics of this detector system, such as light collection in the BGO crystal and response of the electronics, are not significantly different from those of the larger detector.

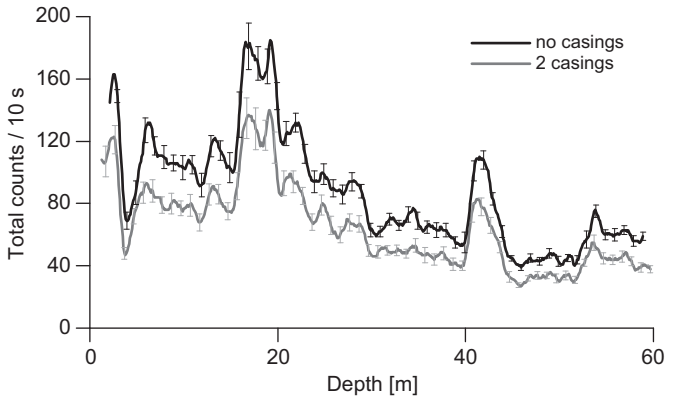

Fig. 12. Total Count rates per 10 s in a borehole in Vollenhove, the Netherlands. Data from two separate measurements are shown. The first measurement is conducted with two steel casings (7.1 and 2.5 mm thick) present in the borehole. The second measurement is performed in the open borehole, after removal of the casings. The data represent a running average over 10 spectra, where each spectrum is accumulated over 1 s at a logging speed of 0.03 m s^{-1}. Statistical uncertainties are given every 100 keV.

lowest-energy γ-radiation is absorbed in the borehole fluid before reaching the small detector; cf. the dip in low-energy flux for the water-filled scenario in Fig. 11.

When comparing the γ-ray spectrum for the water-filled borehole to the vacuum situation, it is important to note that the detector size is not the only difference but also the thickness/amount of surrounding layer of water, which affects properties of transport medium of γ-rays. One notices that the overall intensity is reduced, which is attributed to the γ-ray interactions with the water. Moreover, a strong intensity reduction for $E_\gamma < 100$ keV is observed, due to the absorption of these low-energy γ-rays in the water surrounding the smaller detector. For instance, the intensity of a 20 keV photon beam is reduced by 40% in 0.6 cm water (i.e., water thickness around the ∅3.8 cm detector). For higher γ-ray energies (i.e. $E_\gamma > 500$ keV) the absorption is almost independent of E_γ, an observation holding for borehole fluids of any Z.

5. Experimental validation

In a case study, the simulated standard spectra are experimentally validated. Two data sets (logs) from a 60-m-deep water-filled borehole at Vollenhove, the Netherlands, are analyzed for activity concentrations. In the first measurement, a side-walled system (consisting of 7.1- and 2.5-mm-thick steel casings, Fig. 1) was still present in the borehole. After removal of the steel casings, the second measurement was conducted in the open (uncased) borehole, again with the side-walled system.

Fig. 12 compares the *Total Count* rates for both runs. It is not expected to find a perfect 1-on-1 match between both measurements because the starting points of both runs were not synchronized, causing small mismatches in depth. Moreover, removal of the casings is a process that involves strong forces. As a result, sediment parts can be dislocated and partial collapses of the borehole can occur. Nevertheless, the comparison clearly indicates that the two data sets show similar features, but the γ-ray intensity is significantly lower in the cased configuration. The reduced count rates also affect the statistical uncertainty of the activity concentrations as calculated from the γ-ray spectra.

Both data sets are analyzed in the following ways:

1. Using the same standard spectra for the cased and the open borehole

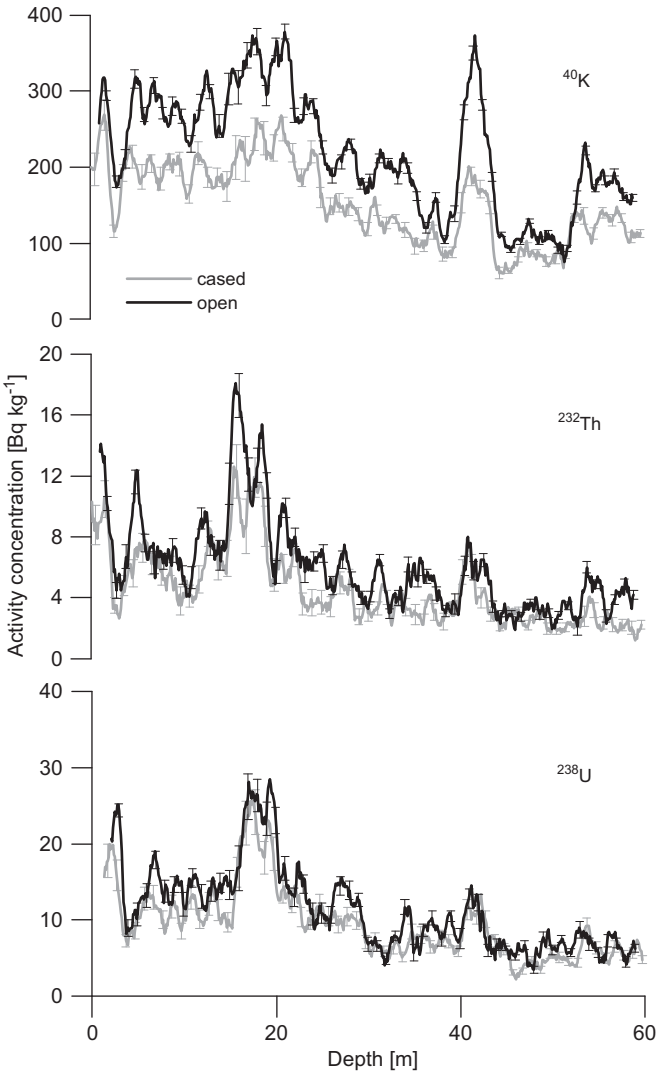

Fig. 13. Activity concentrations of ^{40}K, ^{232}Th and ^{238}U in the Vollenhove borehole, calculated using the standard spectra for uncased boreholes. The γ-ray spectra acquired in open and cased configuration are analyzed using the same set of standard spectra, without correction for the borehole configuration. This approach corresponds to the standard analysis of borehole γ-ray spectra. Statistical uncertainties are given every 100 keV.

These generic standard spectra are measured in a laboratory experiment (i.e. in dry calibration drums at NGD/KVI) for an uncased borehole and used for the analysis of both open and cased configurations, without correcting for borehole configuration. The activity concentration profiles for this analysis given in Fig. 13 indicate that the calculated radionuclide concentrations depend on the measurement configuration. The differences are as high as 50%, emphasizing the need to include the borehole configuration corrections[9] in the analysis. The observed deviations are highest for potassium because the spectral shape of this mono-energetic γ-ray emitter is affected strongest by the γ-ray absorption in casings and fluid and the resulting shift from photo-peak to continuum in the γ-ray spectrum.

[9] The corrections made, using energy-independent factors, correspond to the presence of casings but not to the borehole size and fluid differences with respect to the measured drum standard spectra.

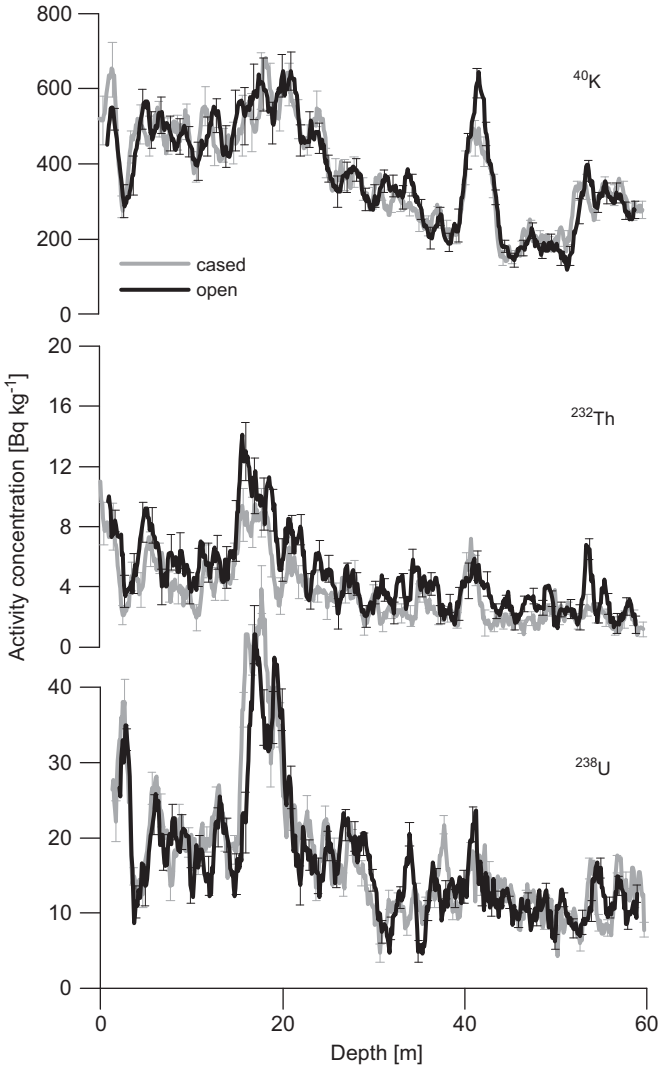

Fig. 14. The activity concentrations of ^{40}K, ^{232}Th and ^{238}U as calculated using two sets of Monte Carlo simulated standard spectra. Each set of standard spectra specifically describes the measuring configuration that was used when the γ-ray spectra were acquired. Statistical uncertainties are given every 100 keV.

2. Using two sets of (simulated) standard spectra, which specifically describe the configurations where the γ-ray spectra are measured
   This analysis therefore represents the situation in which borehole-specific corrections are made. The calculated activity concentrations are given in Fig. 14. Since these spectra take the spectral changes induced by the steel tubing of the side-walled system into account, quantitative results are obtained, and the results should be the same for both measurements. Within the statistical and systematic uncertainties of the experiment, the activity concentrations are identical.

Comparing the concentration profiles from the cased and open measurements as given in Figs. 13 and 14 shows, it is possible to correct for the presence of casings by using standard spectra that specifically describe the configuration. Moreover, the comparison reveals that activity concentrations calculated using the generic (laboratory) standard spectra underestimate the concentrations extracted as found from analysis with simulated standard spectra (note that ranges on the vertical axes in Figs. 13 and 14 are not the same).

The *generic* standard spectra were measured in dry calibration drums at NGD/KVI, with an air-filled borehole of 11 cm diameter, whereas the Vollenhove spectra are acquired in a 15.24-cm-diameter water-filled hole. The energy-independent scaling applied here only corrects for the presence of casings and not for the borehole diameter. Therefore, this example also demonstrates that the activity concentrations depend on borehole diameter. The observed underestimation is as high as 55%. In addition to differences in borehole diameter, this discrepancy can mostly be attributed to (i.e. spectral) differences in scattering and absorption, introduced by the borehole fluid (i.e. water) in experimental borehole vs. air-filled borehole in dry calibration drums.

Rather than using configuration-specific standard spectra to calculate the activity concentrations, one could also have relied on energy-independent correction factors as derived in this manuscript. An advantage of this method is that it is straightforward to apply such corrections after the initial analysis. Additionally, it is possible to apply multiple corrections to the standard spectra. That way, one generic set of standard spectra can be used to which successive corrections are applied until they fully correspond to the actual configuration of the measurement. Given the number of possible borehole configurations, the collection of required standard spectra to describe all configurations is enormous and having adequate correction (“departure”) curves in that case is helpful. This approach, however, neglects coupling between borehole effects, such as *spectrum shifting* associated with fluid (water) attenuation and the energy-dependent *casing attenuation*. For oil-field γ-ray spectrometry, for example, this issue is studied by Mickael et al. [11].

Such behavior is further demonstrated in Figs. 13 and 14, indicating that the activity is erroneously contributed to thorium instead of uranium. This shift is caused by changes in the spectral shape (i.e. *spectrum shifting*) that are not taken into account. As demonstrated in Section 4 of this manuscript, each energy-independent correction increases the systematic uncertainty by roughly 10%. A valid and important conclusion is that if several corrections are combined, the accuracy of determined activity concentrations deteriorates rapidly.

6. Conclusions

Being able to extract, *quantitatively*, the activity concentrations of the natural radionuclides is a requirement for the determination of geotechnical parameters. In turn, quantitative results require that the measurement configuration is included in the data analysis.

To date, nuclide-specific corrections for configuration were unknown for large, high-efficiency γ-ray scintillation detectors, such as BGO or CsI, which employ full-spectrum data analysis. Based on Monte Carlo simulations a catalogue of corrections has been compiled, with results verified in a case study, also presented in this contribution. When no corrections for configuration were applied, the calculated radionuclide concentrations deviated as much as 50%. By using simulated standard spectra describing the specific measurement geometry the activity concentrations were found to be independent of measurement configuration within the statistical and systematic uncertainties of the experiment.

With the corrections derived in this paper, it is now possible to obtain absolute activity concentrations, and therewith formation classifications for a wide variety of common borehole configurations. Furthermore, since the results from measurements in different borehole configurations can now be compared quantitatively, geological interpretations spanning multiple boreholes may become an option.

Acknowledgement

The authors would like to acknowledge assistance of Dr. Everett L. Redmond II for a thorough English-language editing and proofreading of this manuscript.

References

[1] R.J. de Meijer, J. Geochem. Explor. 62 (1998) 81.
[2] L.B. Venema, R.J. de Meijer, J. Environ. Radioact. 55 (2001) 221.
[3] T. Wonik, Paleogeogr. Paleoclimatol. Paleoecol. 174 (2001) 97.
[4] P.H.G.M. Hendriks, J. Limburg, R.J. de Meijer, J. Environ. Radioact. 53 (2001) 365.
[5] M.L. Evans, R.D. Wilson, Calculation of borehole correction factors for gamma-ray spectral logging, Department of Energy Report GJBX-27(83), Grand Junction, CO, 1983.
[6] C.J. Koizumi, J.R. Brodeur, R.K. Price, J.E. Meisner, D.C. Stromswold, Nucl. Geophys. 8 (2) (1994) 149.
[7] D.C. Stromswold, R.D. Wilson, Calibration and data correction techniques for spectral gamma-ray logging, paper M, in: SPWLA 22nd Annual Logging Symposium, Mexico City, Mexico, June 23–26, 1981.
[8] C.J. Koizumi, SPE Formation Eval. 3 (3) (1988) 637.
[9] M.L. Evans, A computer model for calculating gamma-ray pulse-height spectra for logging applications, Los Alamos National Laboratory Unclassified Report, LA-UR-81-400, Los Alamos, NM, 1981.
[10] C.J. Koizumi, J. Appl. Geophys. 61 (2) (2007) 111.
[11] M. Mickael, D. Trcka, R. Pemper, Dynamic multi-parameter interpretation of dual-detector, carbon/oxygen measurements, SPE 56649, in: 1999 SPE Annual Technical Conference and Exhibition, Houston, TX, October 3–6, 1999.
[12] J. Briesmeister (Ed.), MCNP—a general purpose Monte Carlo N-particle transport code version 4C, Report LA-12625-M, Los Alamos National Laboratory, NM, 2000.
[13] R.C. Odom, S.M. Bailey, R.D. Wilson, Appl. Radiat. Isot. 48 (2002) 1321.
[14] R.C. Odom, S.M. Bailey, R.D. Wilson, M.P. Archer, Pulsed neutron density measurements: modeling the depth of investigation and cased-hole wellbore uncertainties, paper JJ, in: SPWLA 40th Annual Logging Symposium, Mexico City, Mexico, May 30–June 3, 1999.
[15] M.W. Michael, A new algorithm for correcting neutron decay logs for boreholes and diffusion effects, paper M, in: SPWLA 40th Annual Logging Symposium, Mexico City, Mexico, May 30–June 3, 1999.
[16] J.H. Young, Spectral gamma-ray (KUT) borehole logging, SPE 9465, in: 1980 SPE Annual Technical Conference and Exhibition, Dallas, TX, September 21–24, 1980.
[17] D.M. Arnold, J. Butler, IEEE Trans. Nucl. Sci. 35 (1) (1987) 844.
[18] Schlumberger, Log Interpretation Charts, SMP-7006, Schlumberger, Sugar Land, TX, 1994.
[19] M. Maučec, P.H.G.M. Hendriks, R.J. de Meijer, Monte Carlo simulation of natural gamma ray spectrometry for underwater surfaces, in: Proceedings of the International Conference on Advanced Monte Carlo for Radiation Physics, Particle Transport Simulation and Applications-MC 2000, Lisbon, Portugal, Springer, 2001, pp. 773–778.
[20] R.L. Grasty, P.B. Holman, Y.B. Blanchard, Transportable calibration pads for ground and airborne gamma-ray spectrometers, Geological Survey of Canada, Paper 90-23, 1991.
[21] P.H.G.M. Hendriks, M. Maučec, R.J. de Meijer, Appl. Radiat. Isot. 57 (2002) 449.
[22] R.B. Firestone (Ed.), Table of Isotopes, 8th ed., John Wiley & Sons, New York, 1996.
[23] P.H.G.M. Hendriks, In-depth γ-ray studies: borehole measurements, Ph.D. Thesis, Rijksuniversiteit Groningen, Groningen, the Netherlands, 2003.
[24] J.S. Schweitzer, Nucl. Geophys. 5 (1991) 65.